# Improved $VO_2$ microbolometers for infrared imaging: operation on the semiconducting-metallic phase transition with negative electrothermal feedback

Carl D. Reintsema, Erich N. Grossman, Jonathan A. Koch

Electromagnetic Technology Division, National Institute of Standards and Technology,
325 Broadway, Boulder, CO 80303

## ABSTRACT

We have investigated the performance of $VO_2$ microbolometers biased on the semiconducting-metal phase transition with negative electrothermal feedback. We deposited crystalline thin films of phase-pure $VO_2$, patterned these films into useful test structures, and evaluated the electrical and optical properties relevant to improved uncooled bolometric sensors. A novel ac-biasing method allows for biasing of the devices on the hysteretic semiconducting-metallic phase transition near 70 °C. Two important advantages result from biasing in the phase transition: high sensitivity, and negative electrothermal feedback (ETF). Under these conditions improvements in speed and noise equivalent power (NEP) are expected. Modest improvements in noise performance and responsivity consistent with simulations were experimentally verified. Our results suggest a large potential performance advantage over current uncooled vanadium oxide sensors which can be realized as either increased bandwidth (faster frame rates) or higher sensitivity.

## 1. INTRODUCTION

There has been much progress over the last several years toward realizing low cost, robust, compact, uncooled thermal imaging systems. The cameras which are being produced today offer impressive performance: net equivalent temperature differences (NETD) as low as 24 mK between adjacent pixels and formats up to 320 x 240 pixels translate directly to unprecedented thermal scene resolution at video frame rates.[1] The best of these systems rely on the temperature dependent resistivity of mixed vanadium oxides in a semiconducting amorphous form, operating at room temperature, as the bolometric sensing mechanism. The key technical breakthroughs which have enabled the technology to reach its current state include engineering of free-standing low-thermal-conductivity membranes (onto which the vanadium oxide is deposited to form a bolometric pixel element), the scale up of this technology to high-fill-factor large-format arrays, and the integration of direct CMOS read out electronics underneath each pixel (for a review of the development and status of this technology see Ref. [2]).

However, the ultimate temperature sensitivity of vanadium oxide, inherent in the semiconducting to metal phase transition of crystalline $VO_2$ slightly above room temperature, has yet to be exploited to further enhance the performance of these types of thermal imaging systems. This effort is analogous in many ways to recent advances in low temperature detectors for low background infra-red and x-ray detection.[3-5] These applications have used the superconducting-metallic phase transition in achieving record sensitivity and noise performance. Furthermore, the phase transitions of many ceramic oxides (including vanadium oxides) have been known for many years.[6] Why has this not been done yet with $VO_2$? The answer lies in the hysteretic nature of the phase transition. The transition occurs at a higher temperature upon warming (which we will hence refer to as the melting branch) than it does upon cooling (the freezing branch). This hysteresis greatly complicates using a sensor thermally biased on the transition. We present a method of operating on this phase transition which could ultimately lead to higher performance IR detection systems.

We use an ac bias to circumvent the hysteresis. The bias heats the sensor completely into the metallic state with each current pulse and then the voltage, which is highly sensitive to incident IR loading, is sampled upon cooling into the transition region. In this manner we recover the enhanced temperature sensitivity of the phase transition. Near the phase transition of crystalline $VO_2$ the resistance can drop more than four orders of magnitude in a temperature span of less then 5 °C. The temperature coefficient of resistance for semiconducting vanadium oxides is typically reported to be $\alpha = 1/R \cdot dR/dT = -2$ to $-6$ %/°C near room temperature. While this is substantially better then conventional metal or semi-metal (such as bismuth) bolometers which offer 0.2 to 0.4 %/°C, a comparable parameter extraction from the midpoint of the transition of one of our

Contribution of U. S. Government, not subject to copyright.

$VO_2$ sensors yields a value up to two orders of magnitude larger, 200 %/°C. This figure of merit is key in extrapolating overall bolometer performance. In addition, the phase transition occurs at a convenient temperature (near room temperature) which lends itself well to biasing in negative electrothermal feedback.

When considering the behavior of a bolometer, the Joule heating of the sensor due to the bias must be accounted for. A bolometer under bias will equilibrate at an elevated temperature relative to its surroundings. This equilibrium operating point is reached when the Joule heating balances the heat loss to the surroundings. Electrothermal feedback (ETF) refers to the interaction between the bias and signal or noise power. ETF is a well known and proven phenomenon and is thoroughly documented in the literature.[2,3,7] Conceptually, it is relatively simple to understand: if the bias is such that an upward thermal fluctuation, which is accompanied by a decrease in the sensor resistance (for negative $\alpha$), causing a reduction in Joule heating at the sensor, then negative feedback occurs. Under negative ETF, the bias acts as a restoring force to return to thermal equilibrium. For a $VO_2$ sensor that has a large negative $\alpha$, a current bias provides negative ETF. The strength of the feedback can be parameterized by the value $\beta$, which is effectively the open-loop gain of the feedback. $\beta$ can be approximately expressed in physical terms relative to the sensor and self-bias conditions as

$$\beta = \alpha \Delta T = \frac{\left(T - T_{base}\right)}{R} \frac{dR}{dT}. \tag{1}$$

Hence high $\alpha$ in combination with a thermal self bias well above the base temperature results in strong negative ETF. $\beta$ can also be extracted from a measurement of the V(I) characteristic of a sensor as

$$\beta = \frac{Z - R}{Z + R}, \qquad Z = \frac{\partial V}{\partial I}, \tag{2}$$

which approaches a maximum as the differential resistance becomes equal and opposite to the dc device impedance. There are several significant advantages which result from strong negative ETF, the most important being 1/f and Johnson noise suppression. Speed enhancement and increased immunity to base temperature fluctuations also result. The main focus of this work was aimed at experimentally realizing both high sensitivity (increased $\alpha$) from operating in the transition and strong negative ETF (high $\beta$) due additionally to self biasing in the transition (from room temperature). Table 1 summarizes these advantages in the extreme negative ETF limit and compares them to a device operated with negligible feedback.

| parameter | $\lvert\beta\rvert \ll 1$ | $\lvert\beta\rvert \gg 1$ |
|---|---|---|
| relative ETF | negligible | strong |
| responsivity (V/W) | $\frac{\beta}{I}$ | $\frac{1}{I}$ |
| $\tau$ (s) | $\tau_0 = \frac{C}{G}$ | $\tau_{eff} = \tau_0 \frac{1}{(1-\beta)}$ |
| $V_N$ ($V/Hz^{1/2}$) (Johnson, 1/f) | $V_{N0}$ | $V_N = V_{N0} \frac{1}{(1-\beta)}$ |
| $\frac{dR/dT}{dR/dT_{base}}$ | 1 | $\frac{1}{\beta}$ |

Table 1 – Extreme negative electrothermal feedback advantage (*I* is the current bias, *C* the sensor heat capacity, and *G* the thermal conductance).

## 2. DEVICE FABRICATION AND DESIGN

The main challenges associated with fabricating useful high performance bolometric sensors included: optimizing film growth to yield sensors with high $\alpha$, determining methods to pattern these films without degradation of their electrical properties, and mitigating the detrimental effects of high contact resistance between overlying metallization and the $VO_2$ films.

| Growth Parameter | Value |
|---|---|
| $T_{substrate}$ | 575 °C |
| $P_{total}$ | 1.00 Pa |
| $P_{O2}$ | 0.21 Pa |
| $P_{ar}$ | 0.79 Pa |
| DC magnetron power | 350 W |
| deposition rate | 90 nm/min |
| nominal deposition time | 2 min |
| nominal film thickness | 180 nm |
| substrate | sapphire ($Al_2O_3$), *c*-cut (0001) |

Table 2 - Standard reactive sputtering film growth parameters.

| Ion Mill Parameter | Value |
|---|---|
| mask | photoresist |
| Ar flow | 8 sccm |
| process pressure | $1.13 \times 10^{-2}$ Pa |
| beam voltage | 300 V |
| beam current | 20 mA |
| accelerator voltage | 300 V |
| probe current density | 0.50 mA/cm$^2$ |
| sample stage | rotating, water cooled |
| $VO_2$ mill rate | ≈ 8 nm/min |

Table 3 – Ion milling process parameters for patterning thin film $VO_2$.

Crystalline thin films of various phases of $V_xO_y$ have been grown by a variety of methods including reactive sputtering,[8-10] reactive electron beam evaporation,[11,12] MOCVD,[13] and pulsed laser deposition.[14] After considering issues such as facilitation, ease, and expense we settled on reactive sputtering as a means of film growth. We adopted initial conditions based on those reported in the literature,[8,12,15] and then proceeded to optimize the film deposition to achieve high quality thin films of $VO_2$ on crystalline sapphire substrates. Ultimately, the process conditions listed in Table 2 were settled on. This process consistently yielded high quality thin films of phase pure, crystalline $VO_2$. The R(T) characteristic of a typical (patterned) sample is shown in Fig. 1. Samples grown under these conditions typically displayed critical temperatures ($T_c$) near 70 °C, hysteresis widths ($T_{c,melt}$-$T_{c,freeze}$) of about 5 °C, and resistance ratios ($R_{60\,°C}/R_{80\,°C}$) in excess of $10^4$.

To pattern the thin films into useful test structures, we used a combination of conventional optical lithography, argon ion milling, and lift off metallization. The detailed parameters for the milling step are listed in Table 3. To reduce contact resistance and promote metal adhesion, the metallization was often preceded by a surface treatment in the contact areas. This treatment involved varying degrees of ion bombardment in the contact areas, both in-situ and ex-situ with respect to the metal deposition. The idea was to effectively create degenerately doped regions in the contacts (through liberation of bound O in the film). Dependent on ion energy and dosage, reduction of contact resistance was observed, but it was often accompanied by degradation of the R(T) characteristics of the film, presumably due to ion induced damage of the film.

The devices we designed, fabricated, and evaluated included three types of structures: sensors of varying geometry with and without resistive heaters in proximity, antenna-coupled microbolometers for optical response measurements, and Van der Pauw structures for measuring specific contact resistance between $VO_2$ and Au. Examples of two of these structures are included as Figs. 2a and 2b.

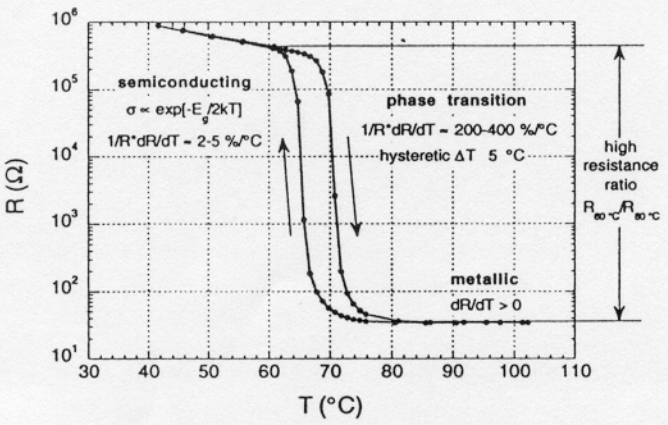


Figure 1 – Typical R(T) of a patterned $VO_2$ device.

The first class of structures included variable sized sensors of $VO_2$ material spanning the range from 1 μm x 1 μm to 300 μm x 300 μm, some with symmetric resistive heating elements as in Fig. 2a. These structures were used primarily for evaluating R(T), V(I), noise, and electrical responsivity. The original goal of this project was to make sensors compatible with a submillimeter wave telecommunication transceiver. To this end, it was necessary to demonstrate quasi-optical coupling of 584 GHz radiation into antenna coupled microbolometers. The device of Fig 2b is such a structure. It is composed of a small (5 μm x 5 μm) $VO_2$ microbolometer at the feed of a 567 GHz resonant double dipole antenna. Radiation from a gas-molecular laser was coupled into this structure

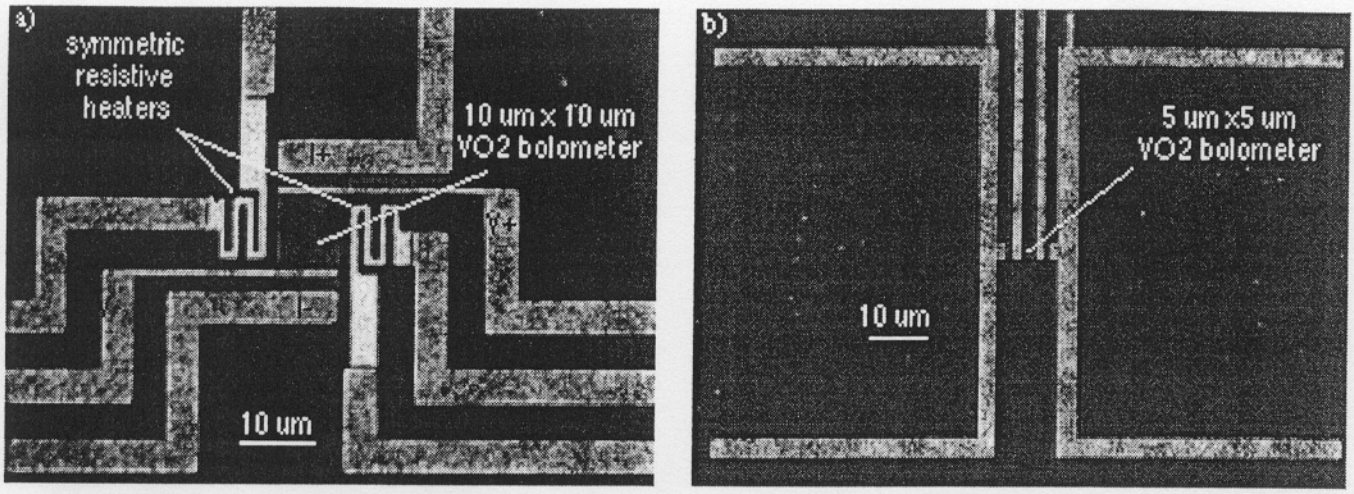


Figure 2 – Photographs of $VO_2$ test structures: (a) 10 μm x 10 μm bolometer with symmetric resistive heating elements and independent V and I leads, (b) 5 μm x 5 μm bolometer at the feed of a double dipole antenna structure resonant for 567 GHz radiation.

through the sapphire substrate by illuminating a hyperhemispherical quartz substrate lens mounted on the backside of the sensor substrate. Van der Pauw structures allowed for simple measurements of the contact resistance between the $VO_2$ and metal films. Various surface treatments and their effect on $\rho_c$ were investigated using these structures. As a final note, all of our test structures were fabricated directly on the sapphire substrate; no effort was made to engineer special thermal isolation structures to enhance performance.

## 3. ELECTRICAL AND OPTICAL CHARACTERIZATION

### 3.1 R(T) characterization

Resistance versus temperature characterizations were routinely undertaken on samples to measure the critical temperature, width, and the hysteresis of the phase transition. There was very little variation observed between samples processed in an identical manner. The critical temperatures (defined as the temperature where the sample is at the midpoint in resistance) were observed to fall in the range of 70-73 °C on the melting branch of the transition and between 65-68 °C on the freezing branch. Outside the transition, semiconducting behavior (conductance $\propto e^{-\Delta T/kT}$) was observed at temperatures below the transition and metallic behavior ($\alpha>0$) was universally observed for temperatures >80 °C. The temperature coefficient of resistance in the semiconducting state was typically in the range of -2 to -6 %/°C. Resistivity in the semiconducting state at room temperature was consistently in the range of 10-20 Ω•cm and dropped to 0.1-1.0 mΩ•cm in the metallic state. All of these properties are plainly displayed in the R(T) of Fig. 1.

Since the main focus of this work was to use sensors biased on the phase transition, significant effort went into evaluation of the transition. Figure 3 shows three high resolution thermal cycles about and within the phase transition for a 3 μm x 3 μm bolometer structure. If a thermal cycle with an excursion greater then the hysteresis width is executed, then the hysteresis loop is closed: the device returns to the original resistance upon cooling. There are two loops in the figure that meet this criterion. If the excursion is less then the transition width a different situation arises. As in the other cases, when the sample is melted, large, continuous, and sometimes discrete reductions in resistance are observed. However, upon freezing, the resistance does not return to the original value; instead it follows a trend consistent with the semiconducting behavior observed below the transition. The main implication of this behavior is that if the sample is dc biased within the transition, the full sensitivity of the transition is not realized: thermal events which cause heating follow the steep melting branch of the R(T) curve but cooling events see only the reduced semiconducting response of the sensor (low $\alpha$). The reason for using an ac bias is to circumvent this restriction.

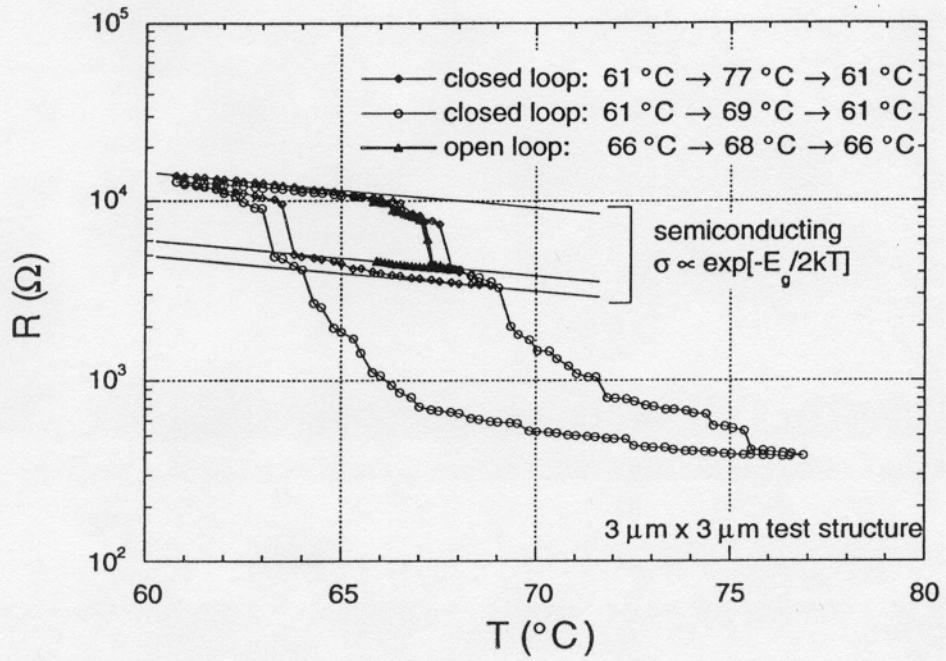


Figure 3 – Local R(T) characteristics for a 3 μm x 3μm bolometer. Three temperature profiles are shown: two which span the transition width and display closed hysteresis loops, and one which spans less then the transition width and results in an open hysteresis loop.

### 3.2 V(I) characterization

Measuring bolometer V(I) curves presented an instrumentation challenge. To maximize the potential benefits of operating in the strong ETF regime, two conditions need to be met: a current bias is required, and the temperature to which the bias self heats the sensor should be as far from the base temperature as practical. For driving a $VO_2$ bolometer this implies the need for a stiff current source with large voltage compliance (so as to act as a current source over the complete range of resistance for the sensor from room temperature to the operating point, 10-$10^5$ Ω). For most measurements we used a custom current source based on a high voltage operational amplifier which was driven and controlled by a standard signal generator.

This issue becomes more apparent upon examination of Fig. 4 which shows the evolution of V(I) as the base temperature is lowered. At the upper left, for a base temperature of 80 °C, the entire sensor is above the transition and in the metallic state. As a result, the device appears entirely resistive (R=100 Ω). As the base temperature is lowered, two features begin to evolve: a region of increased resistance about the origin and the appearance of hysteresis in V(I). The higher resistance is simply the increased resistance at the lower base temperature. The hysteresis is a reflection of the hysteretic R(T) characteristics of the sensor. At the lowest base temperature represented in Fig. 4 (60 °C), the high resistance of the sample in the semiconducting state is clearly evident as the nearly vertical portion of the V(I). Also apparent is a well-defined region of negative differential resistance (Z<0) on the freezing (lower) branch of the V(I) curve. Recalling equation (2), which relates the V(I) to the ETF parameter β, the bias should be selected at the point near where Z approaches –R on the freezing branch for maximum β.

The analogy between the R(T) and V(I) is readily understood using classical bolometer theory. A computer model was developed to compute V(I) from a standard measured R(T) curve. The theory was somewhat limited in applicability due to two fundamental assumptions in the model: no parasitic Joule heating near the sensor and isothermality across the sensor. The first assumption was the more stringent. Simply stated, this assumption implies that all of the heating at the sensor comes from the self-heating due to the bias, P=V*I. The unavoidable parasitic contact resistance rendered this assumption false for most cases; heating at the contacts affected V(I) in a manner not accounted for in the model. The second

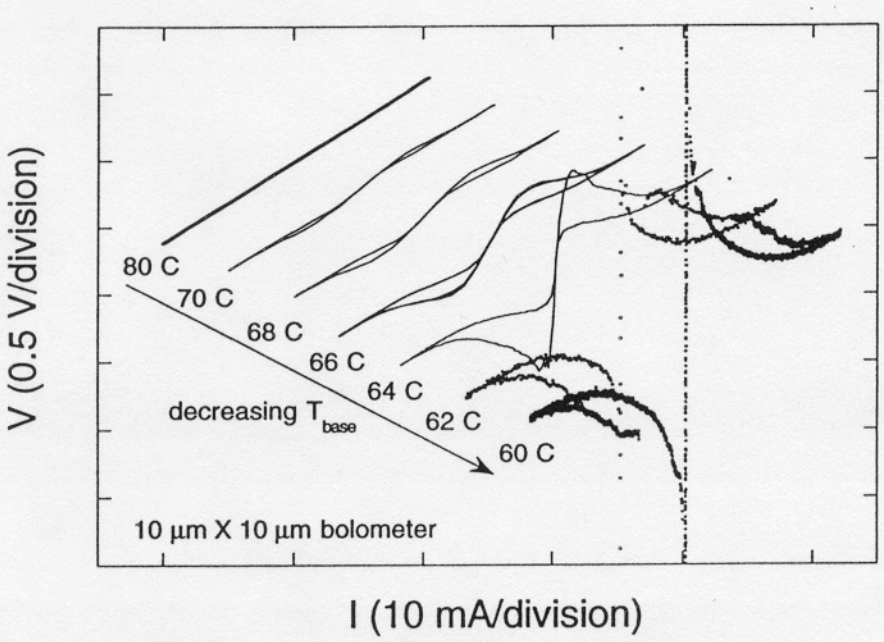


Figure 4 – Evolution of V(I) characteristic as the base temperature is lowered. For clarity, each successive V(I) is offset in I and V. Note the increase in the zero bias resistance (slope at the center of the span), the onset of hysteresis, and the well defined region of negative differential resistance as the base temperature is lowered.

assumption, while not ideal, did not appear to significantly affect the applicability of the model for certain samples. Figure 5 shows V(I), experiment, and theory, for a low resistance sensor with negligibly small contact resistance. The model provides for very good agreement between the V(I) curves for this device.

### 3.3 Bandwidth and noise

The measurement of the time constant (for the same sensor as in Fig. 5) was made by applying a heat pulse to an adjacent heating element and monitoring the response of the sensor. Figure 6 shows such a measurement. An exponential fit to the data provides a measure of the time constant of $\tau$=9 μs. This time constant measurement was made at a dc bias near the foot (R=330 Ω) of the phase transition. The bias point was on the freezing branch (approached from higher temperature by reducing the bias) near $\beta$=0 (the local maximum on lower branch of Fig. 5).

For a conventional bolometer without electrothermal feedback, the response time is simply $\tau_0 = C/G$, where C and G are the heat capacity and thermal conductance of the bolometer. Under dc bias, our bolometers should display a response time close to this value, since the feedback is weak in that case. Because our bolometers have no special thermal isolation structure, the heat capacity is dominated by the volume of substrate material immediately beneath the bolometer; it can be roughly estimated by calculating the heat capacity of a hemisphere of sapphire whose cross-sectional area equals that of the bolometer. For a 10 μm x 10 μm bolometer, this yields C = 1.2 nJ/K. Combining this with the measured thermal conductance (extracted from the V(I) curve) of 380 μW/K yields $\tau_0$ = 3.0 μs. On the other hand, there is another component to the time constant which arises because the $VO_2$ phase transition is first order, with a latent heat that has been measured[16] to be L = 223 J/cm$^3$. This adds an effective heat capacity of $C_{eff} = L/\Delta T$ (where $\Delta T$ is the width of the transition) to the ordinary heat capacity. For a film volume of 10 μm x 10 μm x 0.15 μm and a transition width of 3 K, this implies an additional heat capacity of 1.1 nJ/K, which is (coincidentally) equal to the ordinary component of heat capacity, within the accuracy of the estimates. The expected total capacity is thus approximately 2.3 nJ/K, and the expected time constant is approximately 6.0

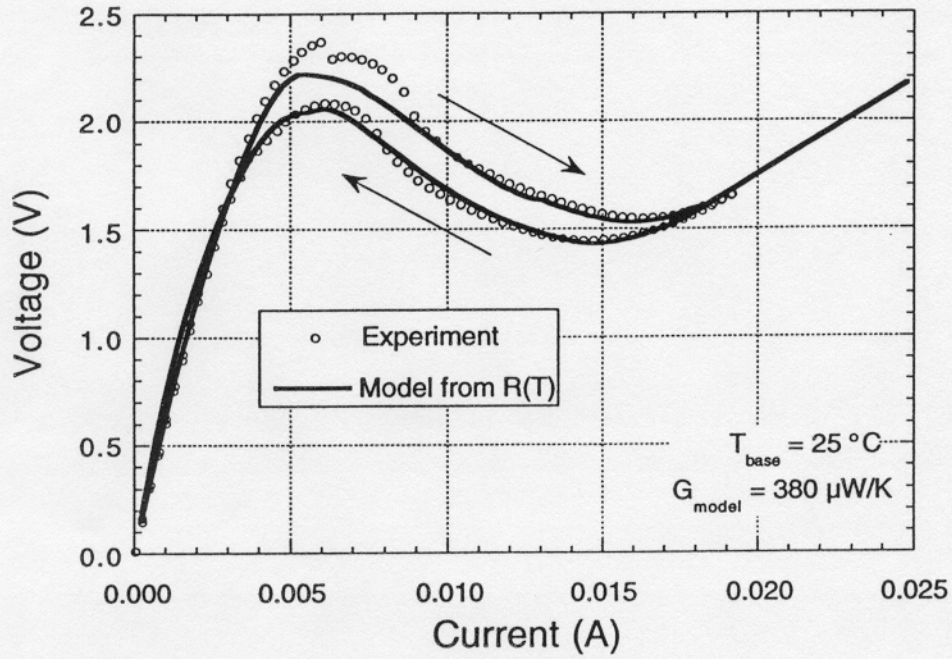


Figure 5 – V(I) experiment versus theory for a low resistance (minimal contact resistance) bolometer.

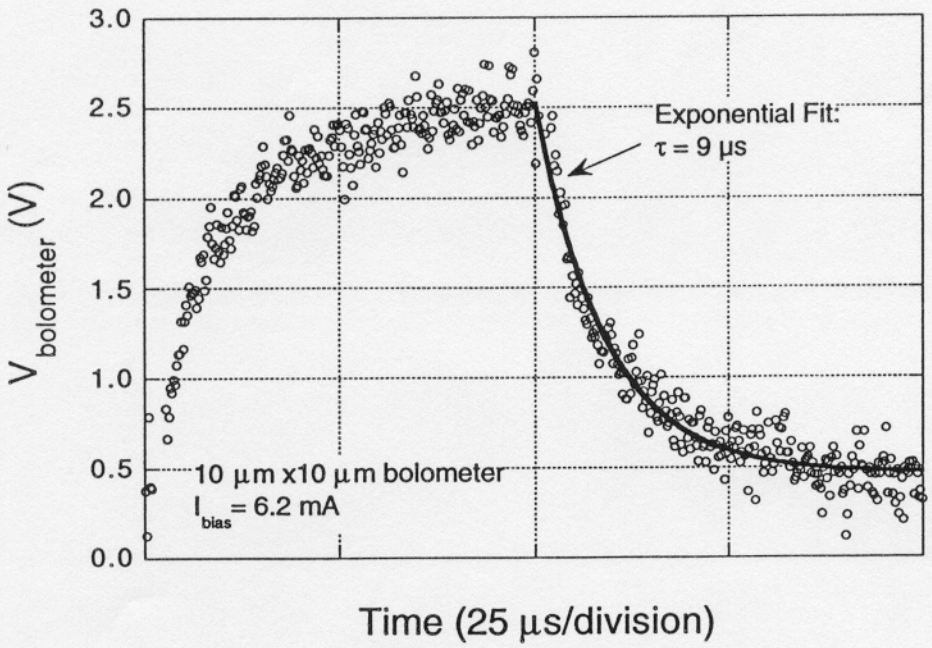


Figure 6 – Bolometer response to electrical heat pulse and extraction of the thermal time constant.

μs. The agreement with our measured time constant of 9.0 μs is quite satisfactory, given the accuracy of the heat capacity estimate.

Voltage noise measurements were made on a variety of devices with differing dc biases. In all cases the bias points were on the freezing branch and approached in the same way as above. The results indicate that for our samples the voltage noise is dominated by 1/f noise at low frequencies. An experiment using dc bias at different thermal bias points was undertaken to evaluate the effect of an ETF bias on the noise properties of the sample. Figure 7 shows the result of this test. The plot shows two noise spectra, one for a base temperature approximately 20 °C above room temperature (46 °C) and the second for a base temperature in the transition (65.8 °C). These two cases correspond to moderate (large $T-T_{base}$) and weak ETF (small $T-T_{base}$). What was observed was a reduction in voltage noise ($V/\sqrt{Hz}$) of –3 dB for the case of higher β. This can be understood considering the hysteresis of the transition and the projections of Table 1: since strong ETF applies only to fluctuations in one direction (high α for melting fluctuations, semiconducting α for freezing fluctuations), only half of the noise is suppressed. This is a direct result of ETF and suggests larger potential noise suppression if a higher effective α can be achieved (circumvent hysteresis through ac biasing schemes). Noise data collected from samples of varying size showed proper volume scaling, $S_V \propto \text{Volume}^{-1}$, over the size range investigated, 3 μm x 3 μm to 100 μm x 100 μm. We also observed the expected bias scaling for resistance fluctuations, $S_R^{V2} \propto R$, over the resistance range of 200 Ω to 3 kΩ.

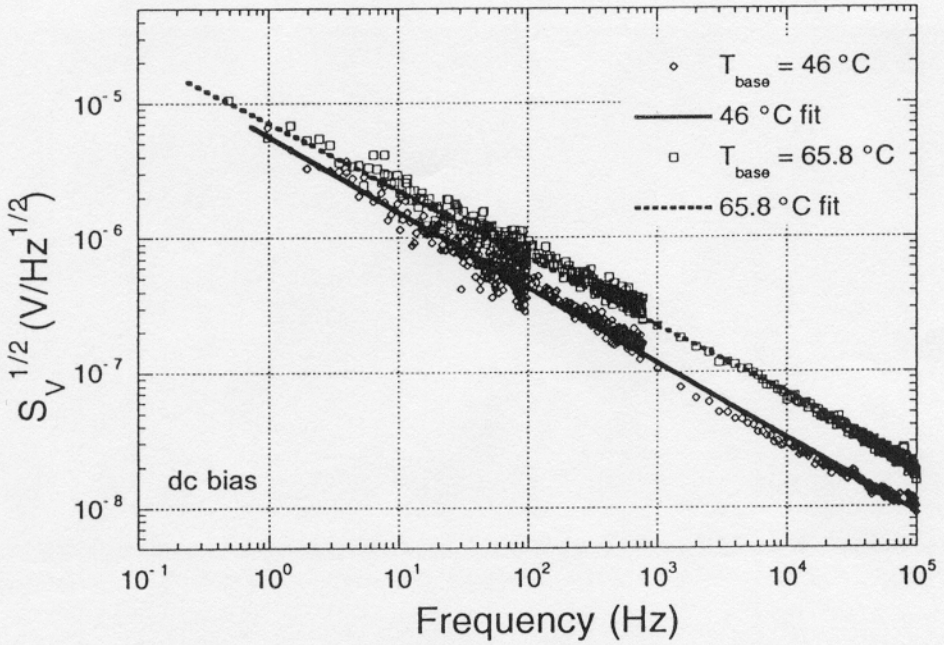


Figure 7 – Voltage noise of dc biased bolometer for moderate ($T_{base}$=46 °C) versus weak ($T_{base}$=65.8 °C) electrothermal feedback.

## 4. OPERATION ON THE HYSTERETIC PHASE TRANSITION

To utilize the hysteretic phase transition, we developed an ac bias scheme which allows for sampling the sensor as it is cooled through the phase transition.[17] We refer to this as correlated double sampling (CDS) due to its similarity to read out methods used in CCD arrays. The idea is to apply an ac bias which resets the sensor by heating it fully above the phase transition once each period and then sample the voltage of the device in the most sensitive region of the V(I) curve as it cools through the transition.

Figure 8 shows the freezing branch of a V(I) curve with and without an external signal (heat pulse into adjacent resistive heater). The offset between the two curves is the signal of interest. Figure 9 shows a schematic of the measurement apparatus and the relevant signals in the time domain. The current drive is a sawtooth whose amplitude and offset is such that at the peak current level the device is self-heated fully into the metallic state and as the current is ramped down, the device cools into the transition. The sensor voltage and heater (signal) voltage are plotted below this. For this proof-of-principle experiment the heater signal was driven at half the current bias frequency so as to cause the sensor to alternately follow the branches of Fig. 8. The lowest timing plot shows the sampling windows during which the sensor voltage is integrated. The windows are referred to as the data and reset windows. During the data window, the sensor is in the transition and the voltage is strongly dependent on the heat loading (optical or electrical). During the reset window, the sensor is metallic and the voltage is (nearly) independent of the heat loading. The signal of interest is then the difference between these two voltage levels. Figure 10 shows the end result. Figure 10 shows the reset voltage, the data voltage, and the difference as functions of time. The lower plot is an enlargement of the difference signal. For the data of Fig. 10, the heat pulse frequency was 15 times lower then the bias frequency hence the difference level changed once for every 15 samples.

The most important conclusion from Fig. 10 concerns the responsivity enhancement observed using the CDS bias technique. The measured responsivity using the ac bias technique was 108 V/W. A direct comparison with data taken under the same conditions only at dc current bias shows an improvement of a factor of 5 using ac bias and CDS. A few comments are in order regarding this result. These data were taken in a region of only modest ETF. The value of $\beta$, extracted directly from the V(I) within the data window, was only -1.36. If we extrapolate an $\alpha$ from this value we find $\alpha$=0.27 $K^{-1}$. We can attribute the responsivity gain to the increased $\alpha$ from operating in the transition ($T-T_{base}$=5 C). If we were able to invoke strong ETF by further increasing $\beta$ (increase $\alpha$ or decrease $T_{base}$), the responsivity would approach the limit of 1/I, which for the case of Fig. 10 is 500 V/W. Beyond the responsivity saturation point, increasing the ETF would continue to suppress Johnson and 1/f noise. In some situations this could lead to an enhanced signal-to-noise ratio (SNR) over a broadened bandwidth. A noise analysis has not been performed for the data of Fig. 10. The peak power at the sampling frequency prohibits the use of a conventional spectrum analyzer for such a measurement. In fact, a qualitative analysis of Fig. 10 suggests a degradation in the SNR. While we do not have sufficient data to fully analyze or verify this result, we suspect that the measurement is limited by the 1/f noise which appears to be worse under ac bias without strong ETF. Further analysis is clearly required.

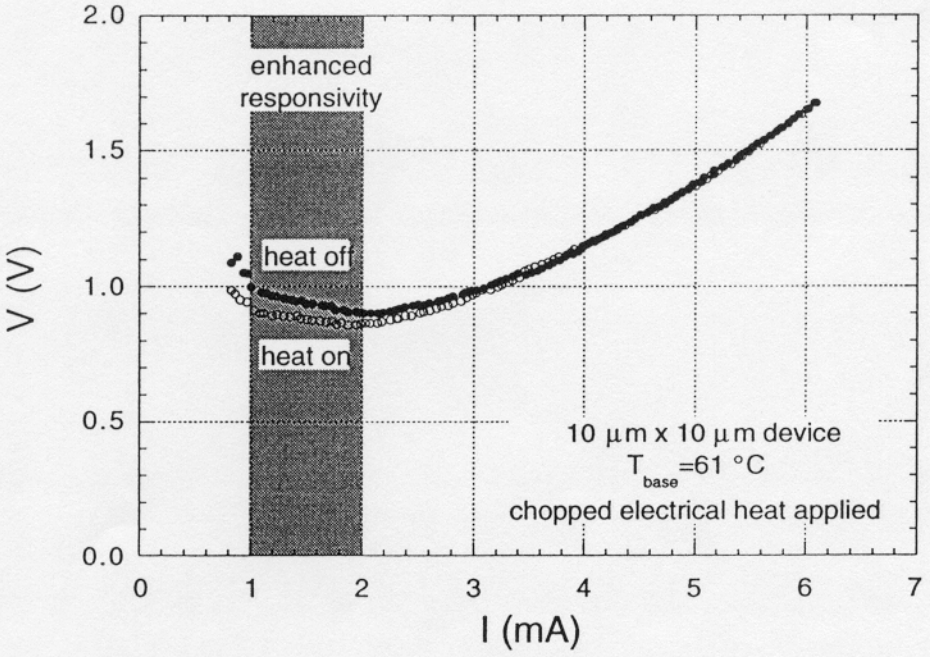


Figure 8 – Local V(I) curve under pulsed electrical heat loading (only the freezing branches are shown).

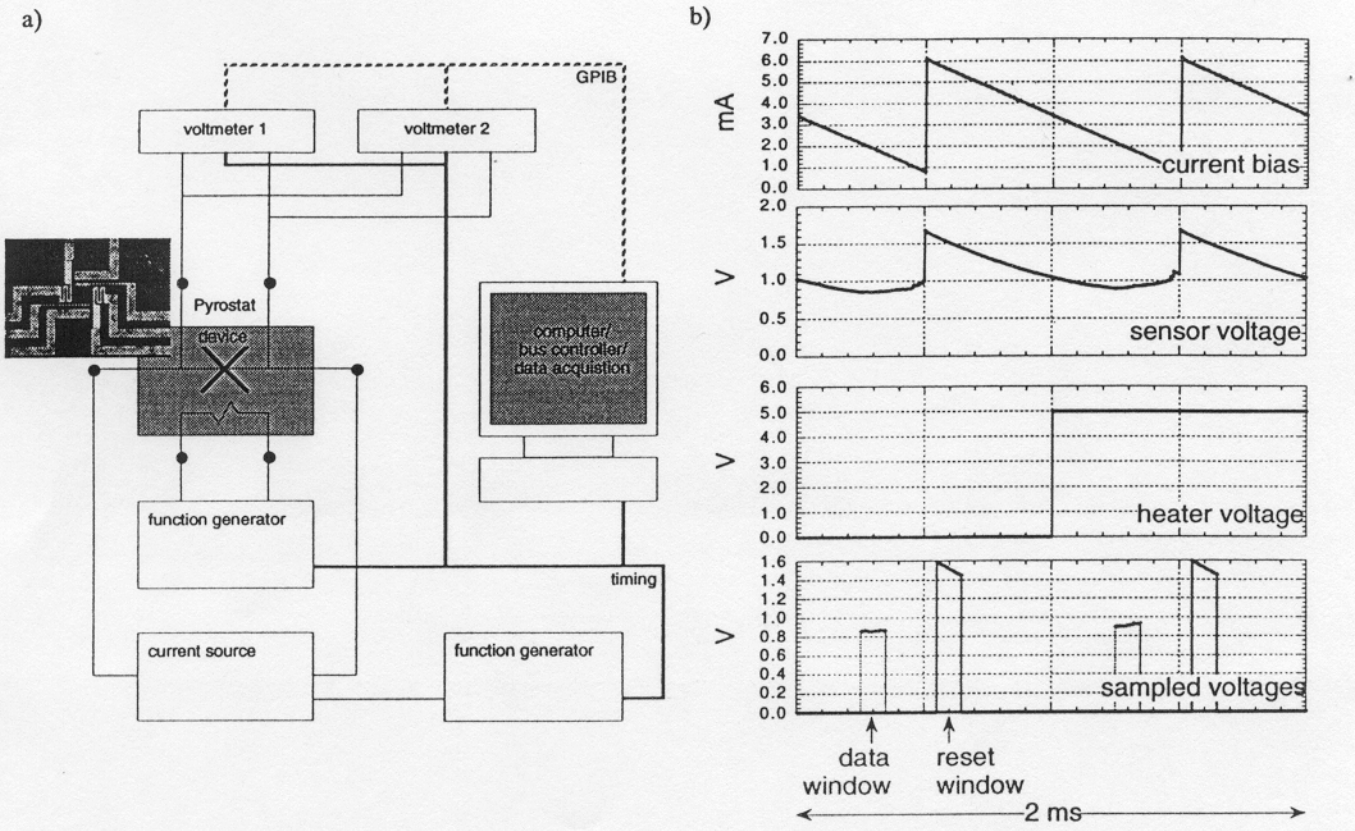


Figure 9 – (a) System diagram for CDS with an ac bias and electrical heat loading, and (b) relevant time domain signals.

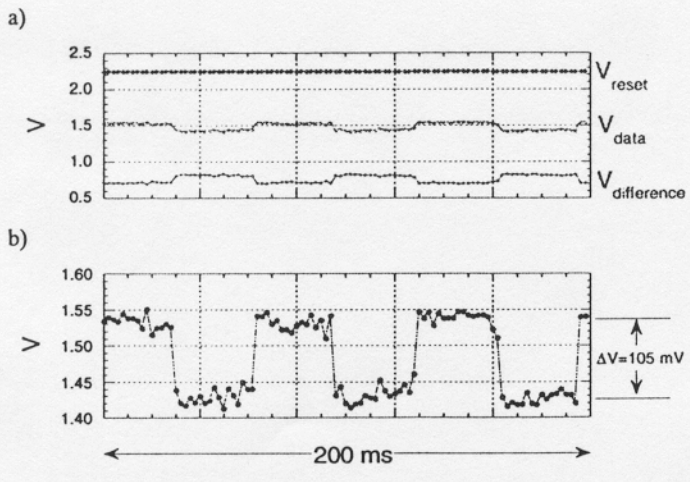


Figure 10 – Measured time domain signals using ac bias and CDS: (a) data, reset, and difference signals, and (b) enlargement of difference signal. Observed responsivity enhancement as compared to dc bias over 5 times.

The convolution of ETF performance gains with benefits inherent to high $\alpha$ sensors is a complex issue beyond the scope of this paper. In a forthcoming publication we intend to cover this topic in detail as it relates to $VO_2$ sensors ac biased in the phase transition. We have, however, performed limited numerical simulations which demonstrate the expected ETF noise suppression for the ac bias case. If strong ETF can be realized with these sensors operating in the transition, then the SNR improvement should lead directly to phonon-noise-limited performance over a wide bandwidth.

## CONCLUSION

Our work with high performance crystalline $VO_2$ microbolometers has shown that the key issues to overcome are the hysteresis of the semiconducting-metallic phase transition and high 1/f noise in the sensors. We have shown that, by using an ac bias technique in combination with CDS readout, the high sensitivity region of the hysteretic phase transition is

accessible. The proof-of-concept measurement discussed in §4 demonstrated an appreciable responsivity enhancement using this technique. However, no noise analysis has been done to evaluate the effect of our bias technique on the SNR or usable bandwidth. Likewise we were unable to determine if the modest negative ETF inherent in our measurement resulted in the expected noise suppression. Furthermore, the experiment of §4 was non-optimal with respect to maximizing $\beta$ for the highest possible performance enhancement ($T_{base}$=30 C and $Z_{bias}$=-R, see Table 1). And more consideration needs to be aimed towards optimizing the bias with respect to waveform shape, amplitude, and frequency. We think that under optimal conditions, significant improvement, comparable with the predictions of Table 1 and $\beta$=100-200, would be observed in single pixels.

Given successful demonstrations of the aforementioned goals, projections based on low thermal conductance pixels (comparable thermal conductance, size, and area to existing arrays) and full recovery of the ETF advantage suggest an appreciable performance improvement when compared to current state of the art (achieving phonon-noise-limited performance with sub-millikelvin NETD). This advantage could be realized in sensitivity (lower NETD) or, since enhanced bandwidth would likely result, traded off for speed (faster cameras, fleeting targets, covert telecommunication).

## ACKNOWLEDGEMENTS

The authors gratefully acknowledge the support of this research under a NSA IDEA grant.

## REFERENCES

1. W. Radford, D. Murphy, A. Finch, A. Kennedy, J. Kojiro, M. Ray, R. Wyles, R. Coda, E. Moody, and S. Baur, "Microbolometer uncooled infrared camera with 20 mK NETD," SPIE **3379**, 22 (1998).
2. R. A. Wood, "Monolithic silicon microbolometer arrays," in *Uncooled Infrared Imaging Arrays and Systems*, edited by Paul W. Kruss and David D. Skatrud (Academic Press, San Diego, 1997), Vol. 47, pp. 43.
3. K. D. Irwin, "An application of electrothermal feedback for high resolution cryogenic particle detection," Appl. Phys. Lett. **66** (15), 1998 (1995).
4. K. D. Irwin, G. C. Hilton, J. M. Martinis, and D. A. Wollman, "X-ray detection using a superconducting transition-edge sensor microcalorimeter with electrothermal feedback," Appl. Phys. Lett. **69** (13), 1945 (1996).
5. A. T. Lee, P. L. Richards, S. W. Nam, B. Cabrera, and K. D. Irwin, "A superconducting bolometer with strong electrothermal feedback," Appl. Phys. Lett. **69** (12), 1801 (1996).
6. F. J. Morin, "Oxides which show a metal-to-insulator transition at the Neel temperature," Phys. Rev. Lett. **3** (1), 34 (1959).
7. J. C. Mather, "Bolometer noise: nonequilibrium theory," Appl. Opt. **21** (6), 1225 (1982).
8. C. H. Griffths and H. K. Eastwood, "Influence of stoichiometry on the metal-semiconductor transition in vanadium oxide," J. Appl. Phys. **45** (5), 2201 (1974).
9. E. E. Chain, "The influence of deposition temperature on the structure and optical properties of vanadium oxide films," J. Vac. Sci. Technol. **4** (3), 432 (1986).
10. H. Jerominek, F. Picard, and D. Vicent, "Vanadium oxide films for optical switching and detection," Opt. Eng. **32** (9), 2092 (1993).
11. F. C. Case, "Improved $VO_2$ thin films for infrared switching," Appl. Opt. **30** (28), 4119 (1991).
12. J. F. De Natale, P. J. Hood, and A. B. Harker, "Formation and Characterization of grain-oriented $VO_2$ thin films," J. Appl. Phys. **66** (12), 5844 (1989).
13. H. K. Kim, H. You, R. P. Chiarello, H. L. M. Chang, T. J. Zhang, and D. J. Lam, "Finite-size effect on the first-order metal-insulator transition in $VO_2$ films grown by metal-organic chemical-vapor deposition," Phys. Rev. B **47** (19), 12900 (1993).
14. D. H. Kim and H. S. Kwok, "Pulsed laser deposition of $VO_2$ thin films," Appl. Phys. Lett. **65** (25), 3188 (1994).
15. K. D. Rogers, J. A. Coath, and M. C. Lovell, "Characterization of epitaxially grown films of vanadium oxides," J. Appl. Phys. **70** (3), 1412 (1991).
16. C. N. Berglund and H. J. Guggenheim, "Electronic Properties of $VO_2$ near the Semiconductor-Metal Transition," Phys. Rev. **183** (3), 1022 (1969).
17. E. N. Grossman and C. D. Reintsema, Provisional Patent Application, USA (Jul 31, 1998).